01

Ion-beam lithography: modelling and analytical description of the deposited in resist energy

© Ya.L. Shabelnikova, S.I. Zaitsev

Institute of Microelectronic Technology Problem and high purity materials, Russian Academy of Sciences,
142432 Chernogolovka, Moscow oblast, Russia
e-mail: janeshabeln@yandex.ru

Received April 25, 2022
Revised April 25, 2022
Accepted April 25, 2022

The energy deposited in resist during its exposure by ion beam was simulated for ions from a set of rare gases and for gallium. It was shown that the distribution of energy density can be approximated by the product of two Gaussian functions. One of them describes the lateral distribution of energy, the second the dependence on depth. The widths and centres of these Gaussian functions are determined by the energy length (also mentioned in the literature as „Range" or „mean length of trajectories"), the mass of ions and the average atomic number of resist. The obtained description would make it possible to estimate the size of the resist modified volume for any type of ion with energy of tens keV. So it can be used for a priori estimates of resolution and performance, as well as for the choice of beam energy and ion type based on this.

Keywords: lithography, nanostructuring, ion beam, resist, modeling, deposited energy.

DOI: 10.21883/TP.2022.08.54550.104-22

Introduction

Miniaturization of integrated circuit elements is still the leading trend in the modern microelectronics technology. It requires constant search for new approaches and improvement of existing lithography methods [1,2]. In this context, ion lithography seems to be one of the most promising methods for achieving nanometer resolution, since for ions the size of the beam with target interaction volume is about tens of nanometers, which is much smaller than that of electrons or UV and X-ray quanta. However, at present the ion beam is mainly used for sputtering the material [3–5] and ion-stimulated deposition [5,6]. These methods are characterized by low energy efficiency. During ion sputtering, only $1-5$ eV [7] of several keV of ion energy is spent on breaking the chemical bonds in substrate, which means the energy efficiency of $\sim 10^{-4}$, even for very high values of the sputtering coefficient $\sim 2-3$ [8,9]. When using an ion beam to deposit liquid or gaseous compounds with their subsequent decomposition, the efficiency is not much higher, since the number of decomposed precursor molecules per ion varies from 2 to 10 [10–13]. Meanwhile, ion lithography based on the exposure of the [14–16] resist should have much higher efficiency together with the high resolution characteristic of ion-beam methods. In this method, the main part of the beam energy is absorbed inside a compact region in the resist and, ultimately, (both for inelastic losses, i.e. ionization of atoms, and for elastic ones, i.e. knocking atoms out of polymer chains) is spent on modification of chemical bonds in resist material.

In this case, the rate of dissolution of the exposed resist is determined by the energy absorbed at a given point, and the power dependence [17,18] is associated with it. Therefore, in order to create methods for restoring the surface of the developed resist from the etching rate and, ultimately, for the theoretical prediction of the sizes and shapes of obtained during the lithographic process structures, it is necessary to develop a description for the absorbed beam energy density which was the purpose of this work.

1. Modeling

The SRIM [19] software package was used to simulate the process of ion deceleration in the resist, which calculates the trajectories using Monte-Carlo method. The output data of this program was processed by means of the program code created in the Matlab package. The resist was divided into layers by depth, and the amount of energy deposited in it was calculated for each layer

$$E(z) = \sum_i S_{ei} L_i + \sum_i E_i, \qquad (1)$$

as a superposition of contributions of electronic (first term) and nuclear (second term) losses. Here S_{ei} and L_i are the electronic stopping power of ion and the length of located in the layer part of rectilinear segment of trajectory. It was taken into account that when modeling trajectories in TRIM, each act of scattering is not processed individually. Instead, it is assumed that at a certain distance, called Free flight distance (after which the ion would be deflected on a fixed angle ($\sim 5^\circ$) due to small-angle scattering), the ion moves in a straight line and loses energy only to the ionization of target atoms (electronic or inelastic losses). At the end of this path, large angle scattering is simulated. Scattering on a large angle corresponds to the interaction of

an ion with an atom as a whole, which leads to so-called nuclear (or elastic) losses. Acts of large angle scattering are most often accompanied by knocking out an atom from the polymer chain, which, in turn, can generate a cascade of displaced atoms. Therefore, the energy E_i transferred to the displaced atom in the cascade was used as an estimate of elastic losses. In the case when the distribution of absorbed energy was estimated without taking into account cascades, the energy of the first displaced atom was used as the E_i. Summation in (1) was carried out for all segments of trajectories located in the layer and all displaced atoms in it.

With respect to the lateral energy distribution, it was assumed that it is centrally-symmetric and is described by a Gaussian function, similar to the energy losses during electron beam deceleration (the justification and derivation of the distribution for electrons can be found, for example, in [20–22]). Further, this assumption was confirmed by modeling. Varying with depth dispersion of this Gaussian function in accordance with the definitions of the second central moment and the dispersion was calculated for each layer as

$$R(z) = \sqrt{\frac{1}{2}\frac{\sum_i r_{ei}^2 Se_i L_i + \sum_i r_i^2 E_i}{\sum_i Se_i L_i + \sum_i E_i}}. \quad (2)$$

Here r_i is the distance from the beam axis to the point of knocking the cascade atom out of the polymer chain, and r_{ei} is the distance from the axis to the middle of the segment L_i. The distances were calculated in a plane perpendicular to the beam axis. Based on this data, the spatial distribution of the absorbed energy density was constructed

$$E(r, z) = \frac{E(z)}{2\pi R^2(z)} \exp\left(-\frac{r^2}{2R^2(z)}\right). \quad (3)$$

Calculations were carried out for the most commonly used in lithography PMMA resist and ions from a set of inert gases (He, Ne, Ar, Kr, Xe, Rn) and for Ga.

2. Analytical description of the absorbed energy distribution

Based on the simulated data, an analytical expression describing the distribution of the absorbed energy density in PMMA was obtained. Calculated dependencies $E(z)$ were analyzed for all considered ion masses and beam energies 5, 10, 20, 30, 40 and 50 keV. It was concluded that the dependence on depth of the energy absorbed in the layer can be described by Gauss function

$$E(z) = A \exp\left(-\frac{(z/L_{energy} - B)^2}{2C^2}\right), \quad (4)$$

whose center and dispersion are proportional to the energy length of the ions L_{energy}. Model curves in comparison with their approximation (4) are shown in Fig. 1, *a* for the beam energy 30 keV. The energy length was determined as the average length of the ion trajectories in resist and calculated according to SRIM data. The coefficients B and C are shown in Fig. 1, *b*. It can be noted that they practically do not change with the atomic number Z and weakly depend on the beam energy. At 30 keV they take the values $B \approx 0.47$, $C \approx 0.38$. For a more accurate description of these coefficients, empirical expressions were derived:

$$B = 1/3 + Z(0.02 - 0.12E/1000)\exp\Big(-0.03Z - 0.73Z\big((E-53)/1000\big)^2\Big), \quad (5)$$

$$C = 1/3 + 0.001Z^{3/2}(6.4 + 0.0023(E-33)^2) \times \exp\Big(-Z\big(83 + 0.0145(E-40)^2\big)/1000\Big), \quad (6)$$

which can be used for energies of 5−50 keV and all atomic masses of ions. As for the lateral Gaussian variance (2), it was shown that it linearly depends on the depth z (Fig. 1, *c*, $E = 30$ keV). The shift and slope of this linear dependence were described by empirical expressions, which include the atomic mass of the ion M and the average atomic mass of the resist M_T, namely

$$R(z) = 11.6\sqrt{\left(\frac{M_T}{M}\right)\left(\frac{E}{30}\right)} + z\,\frac{12M_T}{M + 60M_T}. \quad (7)$$

The discrepancy between the model curves and the empirical description was 0.02−0.2% for $E(z)$ for all ions, and for $R(z)$ it did not exceed 5% for ions heavier than Ne. The discrepancy was calculated as the relative integral standard deviation $\int \big(f_m(z) - f_e(z)\big)^2 dz / \int \big(f_e(z))^2\big) dz$ of model curves $f_m(z)$ from the empirical description $f_e(z)$. In general, a good level of compliance of the empirical description with the simulation results was noted for ions with $Z > 10$. The lightest He ions do not fit into the general scheme, which is apparently due to the predominance of electronic energy losses and, as a consequence, the insignificant influence of cascades on the distribution of absorbed energy (Fig. 1, *d–f*). Indeed, for light ions, the main mechanism of energy loss is inelastic interaction, while for heavy ions, on the contrary, nuclear losses prevail, and electronic losses are insignificant. According to Fig. 1, *d*, it can be seen that in the energy range under consideration, electronic losses are less than 30% for ions heavier than neon, and for ions more massive than argon they do not exceed 15%, rapidly decreasing with increasing atomic number. Fig. 1, *e,f* shows how the absorbed energy is distributed over the depth in the case of helium and gallium, which are examples, respectively, of light and heavy ions. The contributions of electronic and nuclear losses and total energy are also given separately, taking into account and without taking into account cascades of displaced atoms. It can be seen that in the case of gallium, cascades

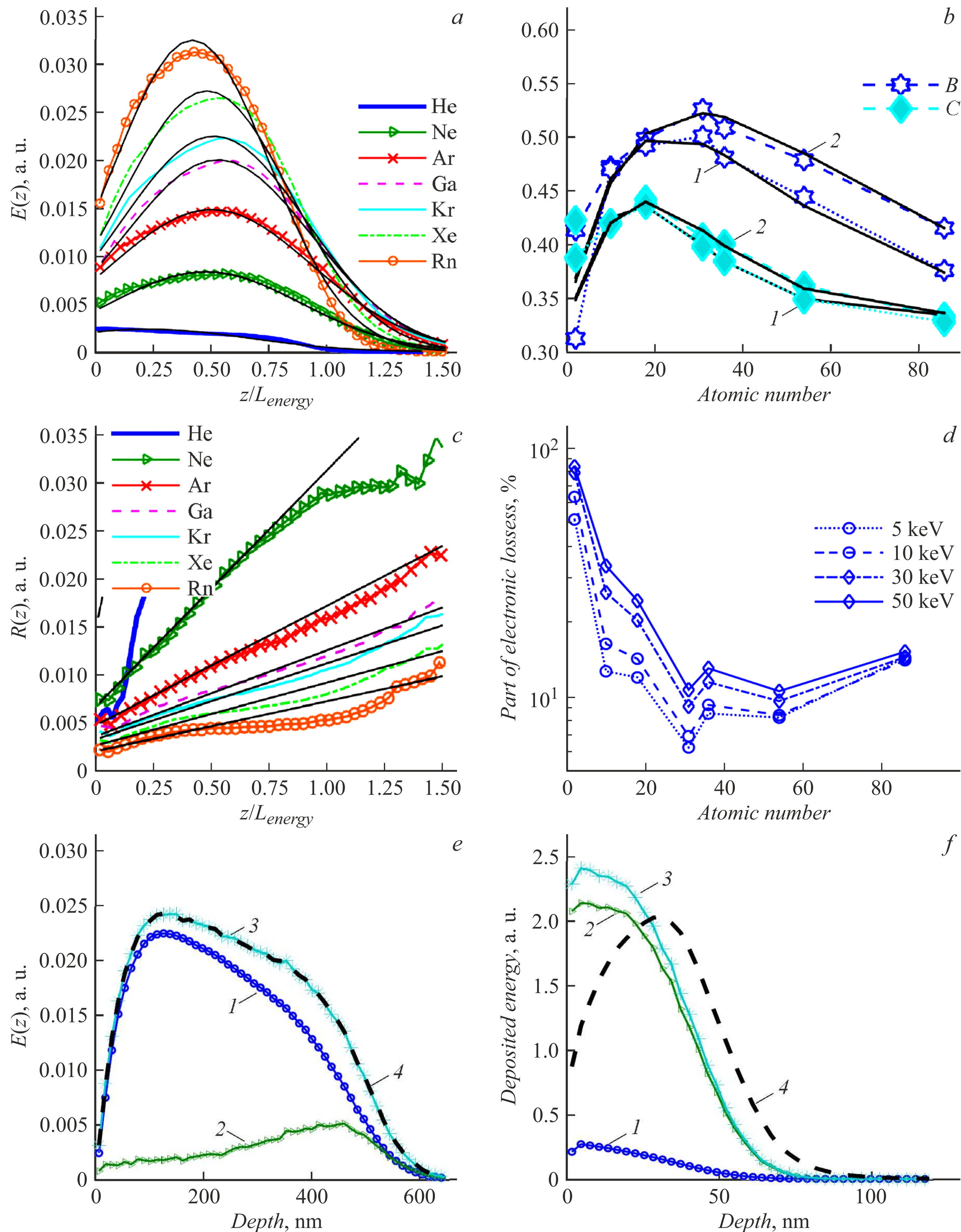

Figure 1. *a* — approximation of $E(z)$ by Gaussian function, *c* — approximation of $R(z)$ by linear dependence. Colored curves are the result of calculation based on trajectories, black ones are the empirical description. *b* — coefficients *B* and *C* for beam energies 10 (*1*) and 30 keV (*2*). The dots show the values obtained from the approximation of $E(z)$, black curves are calculation according to (5) and (6). *d* — the contribution of electronic losses to the absorbed energy depending on the mass and energy of ion. And also for He (*e*) and Ga (*f*) the depth distribution of contributions of electronic (*1*) and nuclear (*2*) losses and total energy without accounting for (*3*) and taking into account (*4*) cascades.

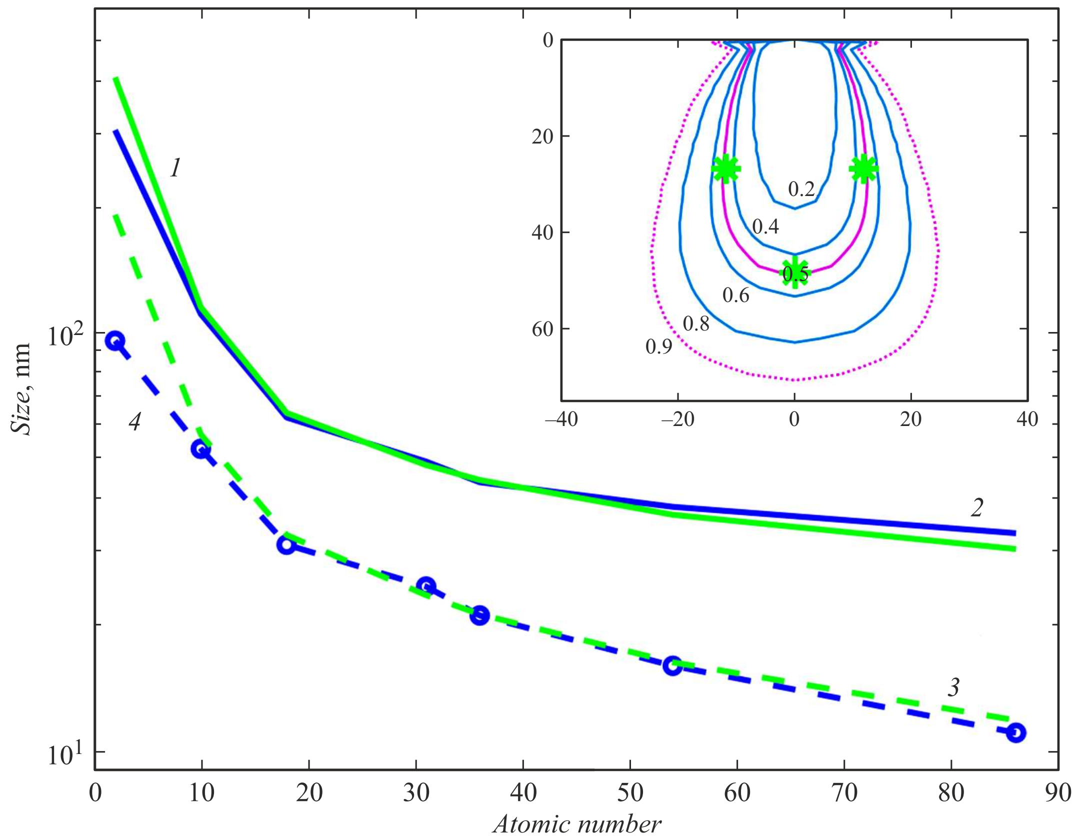

Figure 2. *1, 3* — the dimensions of the modification zone according to the estimation expressions (8) and (9), as well as the depth (2) and width (4) of energy density isosurface, in which half of the total energy is absorbed, depending on the atomic number of the ion. The inset for Ga shows the profiles of isosurfaces with a certain part of total energy (the part is specified as number next to the profile). The points show the sizes (8), (9). Beam energy 30 keV.

significantly redistribute the absorbed energy, forming its maximum at a depth approximately equal to a half the energy length, and creating a characteristic bell-shaped distribution, which is well described by the Gaussian function.

Received description (3)–(7) in the form of a product of Gaussian functions, it allows us to offer easy-to-use estimation expressions for the modified resist volume, as the area in which most of the beam energy is absorbed:

$$D = (B + C)L_{energy}, \tag{8}$$

$$W = 1\left[11.6\sqrt{\frac{M_T}{M}}\left(\frac{E}{30}\right) + (B + C)L_{energy}\,\frac{12M_T}{M + 60M_T}\right]. \tag{9}$$

That is, the depth of the area D is proposed to be estimated as a value one variance away from the maximum of Gaussian distribution (4), and the width W as the doubled variance of the lateral Gaussian $R(z)$ taken at the same depth D.

Fig. 2, in the inset shows the profiles of isosurfaces of energy density, in which a certain proportion (from 20 to 90%) of all energy is absorbed and the sizes of zone (8), (9) are shown. It can be noted that these dimensions are close to the size of the profile with 50% energy.

Analyzing the dependence on the atomic number of D and W (Fig. 2) in comparison with the corresponding sizes of the isosurface containing a half of the energy, it can be noted that these curves have similar dynamics of change and do not differ too significantly. The maximum discrepancy is about 9% for ions heavier than neon. This allows us to assert that inside the region, the dimensions of which are estimated according to (8), (9), for all atomic masses of ions 10–86 and the energy range under consideration, a significant portion of the absorbed energy of the order of 50% will be contained.

Strictly speaking, the specific size of the modification zone is determined by what density of absorbed energy will be enough to dissolve the resist for given conditions of manifestation. However, by varying the exposure dose, it is possible to proportionally increase the absorbed energy, reaching the desired density, but without changing the type of distribution (3)–(7) and the size of the area where all the energy is absorbed (or most of it). It is generally indicates the acceptability of using (8), (9) to estimate the size of the modification zone.

Conclusion

Thus, as a result of approximation of the simulated distributions of the absorbed energy density, an analytical expression for its description is obtained. It can be applied for a wide range of atomic numbers of ions 10−86 and for beam energies of tens keV. It is shown that in this case the mechanism of elastic (or nuclear) stopping is predominant and cascades of displaced atoms significantly affect the final distribution of absorbed energy. Estimation expressions are also proposed to assess the width and depth of the resist modification zone as the area in which half of the total beam energy is absorbed. The obtained theoretical description can be used in order to quickly, without time consuming Monte-Carlo simulations of trajectories, before conducting the experiment, estimate the size of modification zone, and hence both resolution and performance, and based on this, choose the beam energy and the ion−resist pair.

Funding

The study was supported by the State Task № 075-00706-22-00.

Conflict of interest

The authors declare that they have no conflict of interest.

References

[1] *Microlithography Science and Technology, Second Edition*, ed. by K. Suzuki, B.W. Smith. (CRC Press, 2007), p. 864.

[2] K. Lucas, S. Postnikov, C. Henderson, S. Hector. *Lithography: Concepts, Challenges and Prospects*. In *Nano and Giga Challenges in Microelectronics*, ed. by J. Greer, A. Korkin, J. Labanowski (Elsevier, 2003), p. 69.

[3] A. Joshi-Imre, S. Bauerdick. J. Nanotechnology, **2014** (6), 170415 (2014). http://dx.doi.org/10.1155/2014/170415

[4] P. Li, S. Chen, H. Dai, Z. Yang, Z. Chen, Y. Wang, Y. Chen, W. Peng, W. Shana, H. Duan. Nanoscale, **4**, 1529 (2021). https://doi.org/10.1039/D0NR07539F

[5] F.I. Allen. Beilstein J. Nanotechnol., **12**, 633 (2021). https://doi.org/10.3762/bjnano.12.52

[6] S. He, R. Tian, W. Wu, W.-D. Li, D. Wang. Int. J. Extrem. Manuf., **3**, 012001 (2021). https://doi.org/10.1088/2631-7990/abc673

[7] Y. Kudriavtsev, A. Villegas, A. Godines, R. Asomoza. Appl. Surf. Sci., **239**, 273 (2005). https://doi.org/10.1016/J.APSUSC.2004.06.014

[8] J.R. McNeil, J.J. McNally, P.D. Reader. *Ion Beam Deposition*. In *Handbook of Thin-Film Deposition Processes and Techniques — Principles, Methods, Equipment and Applications*, 2nd Edition (William Andrew Publishing / Noyes, 2002), p. 463.

[9] J. Gierak. *Focused Ion Beam Direct-Writing*. In *Lithography*, ed. by S. Landis (Wiley-ISTE, 2010), p. 184.

[10] A.D. Dubner. *Mechanism of Ion Beam Induced Deposition, PhD Thesis* (MIT, 1990)

[11] J. Mengailis. Procc. SPIE, **1465**, 36 (1991). https://doi.org/10.1117/12.47341

[12] J.S. Ro, C.V. Thompson, J. Melngailis. J. Vac. Sci. Technol. B, **12**, 73 (1994). https://doi.org/10.1116/1.587111

[13] A.D. Ratta. *Focused Ion Beam Induced Deposition of Copper, Master's Thesis* (MIT, 1993)

[14] M. Komuro, N. Atoda, H. Kawakatsu. J. Electrochem. Soc.: Solid State Sci. Technol., **126** (3), 483 (1979). https://doi.org/10.1149/1.2129067

[15] R.L. Kubena, J.W. Ward, F.P. Stratton, R.J. Joyce, G.M. Atkinson. J. Vac. Sci. Technol. B, **9** (6), 3079 (1991). https://doi.org/10.1116/1.585373

[16] K. Arshak, M. Mihov, Sh. Nakahara, A. Arshak, D. McDonagh. Superlattices Microstructures, **36**, 335 (2004). https://doi.org/10.1016/J.SPMI.2004.08.030

[17] Ya.L. Shabelnikova, S.I. Zaitsev, N.R. Gusseinov, M.T. Gabdullin, M.M. Muratov. Semiconductors, **54** (14), 1854 (2020). https://doi.org/10.1134/S1063782620140262

[18] M.M. Muratov, M.M. Myrzabekova, N.R. Guseinov, R. Nemkayeva, D.V. Ismailov, Ya.L. Shabelnikova, S.I. Zaitsev. J. Nano-and Electron. Phys., **12** (4), 40038 (2020). https://doi.org/10.21272/jnep.12(4).04038

[19] J.F. Ziegler. *SRIM — the Stopping and Range of Ions in Matter*, 2013. http://www.srim.org

[20] K. Vutova, G. Mladenov. J. Optoelectron. Adv. Mater., **10**, 233 (2008).

[21] G. Mladenov, K. Vutova, I. Raptis, P. Argitis, I. Rangelow. Microelectron. Eng., **57**−**58**, 335 (2001). https://doi.org/10.1016/S0167-9317(01)00521-4

[22] K. Vutova, G. Mladenov. *Computer Simulation of Processes at Electron and Ion Beam Lithography, Part 1: Exposure Modeling at Electron and Ion Beam Lithography. In Lithography*, ed. by M. Wang (IntechOpen, London. 2010), https://doi.org/10.5772/8183